Title: ATP disrupts lipid binding equilibrium to drive retrograde transport critical for bacterial outer membrane asymmetry

Authors: Wen-Yi Low[a], Shuhua Thong[a], Shu-Sin Chng[a,b,*]

Affiliations:

[a] Department of Chemistry, National University of Singapore, Singapore 117543.

[b] Singapore Center for Environmental Life Sciences Engineering, National University of Singapore (SCELSE-NUS), Singapore 117456.

* To whom correspondence should be addressed. Email: chmchngs@nus.edu.sg

Abstract

The hallmark of the Gram-negative bacterial envelope is the presence of the outer membrane (OM). The OM is asymmetric, comprising lipopolysaccharides (LPS) in the outer leaflet and phospholipids (PLs) in the inner leaflet; this critical feature confers permeability barrier function against external insults, including antibiotics. To maintain OM lipid asymmetry, the OmpC-Mla system is believed to remove aberrantly localized PLs from the OM and transport them to the inner membrane (IM). Key to the system in driving lipid trafficking is the MlaFEDB ABC transporter complex in the IM, but mechanistic details, including transport directionality, remain enigmatic. Here, we develop a sensitive point-to-point in vitro lipid transfer assay that allows direct tracking of [^{14}C]-labelled PLs between the periplasmic chaperone MlaC and MlaFEDB reconstituted into nanodiscs. We reveal that MlaC spontaneously transfers PLs to the IM transporter in an MlaD-dependent manner that can be further enhanced by coupled ATP hydrolysis. In addition, we show that MlaD is important for modulating productive coupling between ATP hydrolysis and such retrograde PL transfer. We further demonstrate that spontaneous PL transfer also occurs from MlaFEDB to MlaC, but such anterograde movement is instead abolished by ATP hydrolysis. Our work uncovers a model where PLs reversibly partition between two lipid binding sites in MlaC and MlaFEDB, and ATP binding and/or hydrolysis shift this equilibrium to ultimately drive retrograde PL transport by the OmpC-Mla system. These mechanistic insights will inform future efforts towards discovering new antibiotics against Gram-negative pathogens.

Introduction

The cell envelope of Gram-negative bacteria is composed of two lipid bilayers. The inner membrane (IM) is a phospholipid (PL) bilayer while the outer membrane (OM) contains both PLs and lipopolysaccharides (LPS). The OM is asymmetric with LPS residing in the outer leaflet and PLs in the inner leaflet; such lipid asymmetry allows the membrane to function as an effective barrier against the entry of toxic substances, including antibiotics (1, 2). Extensive efforts have contributed towards an improved understanding of the molecular mechanisms involved in OM assembly and homeostasis. We now know that the Lol, Bam, and Lpt pathways are responsible for the unidirectional transport and/or assembly of OM lipoproteins, β-barrel proteins and LPS, respectively (3-5). However, mechanisms for PL transport (6), which occur in both directions for assembly and homeostasis of the OM (7-9), remain largely elusive.

The first pathway implicated in bacterial PL transport is the OmpC-Mla system (10, 11). Cells lacking this pathway accumulate PLs in the outer leaflet of the OM, indicating a role in the maintenance of OM lipid asymmetry. The OmpC-Mla system is believed to mediate retrograde PL transport where the periplasmic MlaC chaperone shuttles PLs from the OmpC-MlaA complex in the OM to the MlaFEDB ATP-binding cassette (ABC) transporter in the IM. MlaA is an OM lipoprotein that interacts and works with trimeric osmoporin OmpC (11, 12), but forms a separate hydrophilic channel in the OM for trans-bilayer PL translocation (12, 13). MlaC is found to bind PLs with high affinity in a deep hydrophobic pocket (14-16), presumably enabling extraction of PLs from the OM via OmpC-MlaA. In the IM ABC transporter, MlaE and MlaF constitute the permease and nucleotide binding domains, respectively. MlaD is a substrate-binding protein containing a single transmembrane helix, and its periplasmic MCE domain (17) forms a hexamer with a hydrophobic pore and co-purifies with PLs (14, 18). Recent structural studies of the MlaFEDB complex revealed that the MlaE permease domains complement the MlaD hydrophobic pore to form a contiguous cavity for binding and transporting PLs (19-23). MlaB is a cytoplasmic protein containing the STAS domain (24), and has been shown to be essential for the proper assembly and activity of the IM complex (18, 25). How ATP hydrolysis may drive PL movement within the MlaFEDB complex is not known.

Apart from the lack of mechanistic details, there is still substantial controversy with regards to the directionality of lipid transport mediated by the OmpC-Mla system. Genetic studies in *Escherichia coli* and *Acinetobacter baumannii* are more consistent with the retrograde (OM-to-IM) model (10, 26). In particular, *E. coli mla*

54 or *ompC* mutants accumulate outer leaflet PLs in the OM, a phenotype that can be corrected by overexpression of
55 PldA, the OM phospholipase (15, 16). In addition, *A. baumannii* strains lacking lipooligosaccharides (LOS) have
56 enhanced growth and restored OM barrier function when the Mla system and PldA are removed, presumably because
57 these cells need enough PLs to maintain the outer leaflet of the OM (26, 27). Nevertheless, these experiments in
58 cells lack evidence that demonstrate the direct transport of PLs. While there was a report suggesting the system in
59 *A. baumannii* may be involved in anterograde (IM-to-OM) PL transport (28), it has recently been shown that the *mla*
60 mutant strains used had secondary mutations in them, thus rendering the claim invalid (29). A key experiment that
61 sheds light on transport is when the overexpression of MlaFEDB together with MlaC partially rescued defects in
62 retrograde transport of PLs, observed in *E. coli* strains lacking the Tol-Pal complex (30). Despite this, however, in
63 vitro reconstitution demonstrated ATP-independent (anterograde) transfer of PLs from MlaFEDB complex (in
64 liposomes) to MlaC (31). These conflicting data throw into question the biological significance of ATP hydrolysis and
65 argue for the need to provide additional in vitro evidence to truly define the directionality of lipid transport mediated
66 by the OmpC-Mla system.

67 In this study, we utilize [^{14}C]-labelled lipids to directly track the point-to-point transfer of PLs between MlaC
68 and nanodisc-reconstituted MlaFEDB complex. We show that PLs bound to MlaC can be spontaneously transferred
69 to MlaFEDB in an MlaD-dependent manner. The presence of ATP further enhances such retrograde transfer; we
70 demonstrate that ATP hydrolysis is coupled to PL transport, and this process too is modulated by MlaD. Interestingly,
71 spontaneous PL transfer can also happen from MlaFEDB to MlaC, but ATP hydrolysis prevents this 'anterograde'
72 transfer, ultimately driving PL transport in the retrograde direction. Our work establishes that the OmpC-Mla system
73 powers the retrograde transport of PLs via ATP hydrolysis to maintain OM lipid asymmetry.

74

75 **Results**

76 **MlaD stimulates the ATP hydrolytic activity of MlaFEB in a native lipid environment**

77 To gain insights into the directionality of PL transport mediated by the OmpC-Mla system, we focused on
78 lipid transfer between MlaC and the MlaFEDB complex embedded in a lipid bilayer. We first reconstituted MlaFEDB
79 and MlaFEB complexes into lipid nanodiscs stabilized by the membrane scaffold protein MSP1E3D1 (Figure 1A)
80 (32), and tested their functionality in ATP hydrolysis. At room temperature, the ATPase activity of nanodisc-

81 embedded MlaFEDB was drastically reduced compared to that of the same complex solubilized in detergent micelles
82 (Figure S1A, k_{cat}: 0.029 ± 0.002 vs 0.126 ± 0.008 μmol ATP s^{-1}/μmol complex, respectively), likely due to higher
83 conformational restriction within the membrane. At physiological temperature (37°C), however, this activity was
84 largely recovered in the nanodisc-embedded complex (k_{cat}: 0.090 ± 0.002 μmol ATP s^{-1}/μmol complex). In contrast
85 to complexes in detergent micelles (18), we further showed that the ATPase activity of nanodisc-embedded MlaFEDB
86 was much higher than that of MlaFEB (k_{cat}: 0.011 ± 0.002 μmol ATP s^{-1}/μmol complex) at 37°C (Figure 1B). In
87 addition, this activity remained unaffected upon addition of holo- (PL-bound) or apo- (PL-free) MlaC (Figure S1B).
88 Therefore, the presence of MlaD actually stimulates the ATP hydrolytic function of MlaFEB, consistent with MlaD
89 being the substrate binding protein in direct contact with the ABC transporter.
90
91 **MlaC transfers PLs to MlaFEDB in spontaneous and ATP-enhanced manners in vitro**
92 We next tested the possibility of retrograde transport and investigated whether nanodisc-embedded
93 MlaFEDB is able to abstract and receive PLs from MlaC at 37°C. We incubated tag-less MlaC bound to [^{14}C]-labelled
94 PLs (Figure S2A and S2B) with His-tagged MlaFEDB complex in non-labelled nanodiscs, and monitored transfer of
95 radioactive lipids following optimal nickel affinity-based separation of the two components (Figure 2A and S2C). The
96 nanodisc-embedded MlaFEB complex lacking MlaD was used as control; with or without ATP, a small amount of
97 radioactive PLs on MlaC was transferred to the MlaFEB nanodiscs and treated as 'non-specific' background (~11%)
98 (Figure 2B). Interestingly, we observed a substantial increase in spontaneous transfer of radioactive PLs from MlaC
99 to nanodiscs when MlaD was present in the complex (~28% with background subtracted) (Figure 2B). Following
100 activation with ATP, even more PLs were transferred to the MlaFEDB complex (~41% with background subtracted;
101 ~1.5 fold above the level without ATP) (Figure 2C). Importantly, both the spontaneous and ATP-enhanced gains in
102 radioactive PLs on the nanodiscs were accompanied by corresponding losses from MlaC (albeit with ~10-15%
103 radioactivity unrecovered), overall indicating point-to-point PL transfer (Figure 2B). We have therefore reconstituted
104 MlaD- and ATP-dependent retrograde PL transport from MlaC to the IM ABC transporter in vitro.
105
106
107

108 **ATP hydrolysis by the MlaFEDB complex is coupled to retrograde PL transport**

109 We next characterized the observed ATP-enhanced PL transfer from MlaC to nanodisc-embedded
110 MlaFEDB. Mutations in K47 in the Walker A motif of MlaF and in the conserved T52 residue in MlaB have been
111 reported to abolish ATP hydrolytic activity of the ABC transporter in detergents (18). We showed that the Walker A
112 $MlaF_{K47A}$ variant, which is unable to hydrolyze ATP in nanodiscs (Figure 3A and S3A), still allowed spontaneous PL
113 transfer from MlaC to $MlaF_{K47A}EDB$, but completely abolished ATP-enhanced transfer (Figure 3B and S3B). In
114 addition, either the use of the non-hydrolyzable ATP analog, AMP-PNP (Figure 3C and S3C), or the ATPase inhibitor,
115 vanadate (Figure 3D, S3D and S4), similarly led to the loss of ATP-activated PL transfer from MlaC to wildtype
116 MlaFEDB, establishing that ATP hydrolysis is required for this process. Consistent with this idea, complexes with the
117 $MlaB_{T52A}$ variant (18), which we now show possesses partial ATPase activity in nanodiscs (Figures 3A and S3A),
118 exhibited correspondingly lower ATP-enhanced PL transfer from MlaC (Figure 3B and S3B). We further
119 demonstrated that the amount of radioactive PLs recovered on wildtype MlaFEDB nanodiscs reached a plateau with
120 increasing concentrations of ATP (Figure 3E and S3E), establishing that ATP-activated PL transfer is saturable and
121 thus specific. In fact, the K_M for ATP in enhanced PL transfer activity (33.1 ± 22.2 μM) is comparable to that in ATPase
122 activity of the complex (70-83 μM across multiple experiments). We conclude that ATP hydrolysis is strongly coupled
123 to retrograde PL transport mediated by the IM Mla complex.

124

125 **MlaD modulates PL lipid binding capacity and ATP hydrolytic activity of the MlaFEDB complex in retrograde**
126 **PL transfer**

127 We next went on to investigate the role of MlaD, especially given that it is required for the transfer of PLs
128 from MlaC to the MlaFEDB complex in the absence of ATP. To do that, we examined two non-functional MlaD
129 variants that have previously been reported ($MlaD_{L106N/L107N}$ and $MlaD_{\Delta141-183}$) (14). The L106N/L107N mutation is
130 found at one of the constriction points of the central hydrophobic pore of MlaD hexamers, while the Δ141-183 deletion
131 removes the C-terminal helices that form part of the pore; both are expected to affect lipid binding of the complex. In
132 addition, $MlaD_{\Delta141-183}$ forms hexamers in the complex that are no longer SDS-resistant, exhibiting lower stability than
133 those of wildtype MlaD and $MlaD_{L106N/L107N}$ (Figure S5). Indeed, we observed elevated or reduced spontaneous
134 transfer of radioactive PLs from MlaC to nanodisc-embedded $MlaFED_{L106N/L107N}B$ (~1.3-fold) or $MlaFED_{\Delta141-183}B$ (~0.7-

135 fold, compared to wildtype MlaFEDB), respectively (Figure 4A and S6A). As expected, MlaD directly modulates the
136 PL binding capacity of the MlaFEDB complex.

137 Interestingly, these MlaD mutations also affected the ATP hydrolytic activities of the corresponding
138 complexes. The MlaFED$_{L106N/L107N}$B complex exhibited reduced ATPase activity (Figure 4B and S6B) and hence had
139 much lower ATP-enhanced PL transfer from MlaC (Figure 4A and S6A). Remarkably, the MlaFED$_{\Delta 141\text{-}183}$B variant
140 displayed much greater ATPase activity than wildtype complex (Figure 4B and S6B), yet was unable to activate
141 additional PL transfer in the presence of ATP (Figure 4A and S6A). We conclude that MlaD modulates ATPase
142 function and is essential for coupling ATP hydrolysis to PL transfer in the MlaFEDB complex.

143

144 **ATP hydrolysis prevents spontaneous transfer of PLs from MlaFEDB to MlaC**

145 We have now established that MlaC spontaneously transfers PLs to the MlaFEDB complex in a manner that
146 can be enhanced by ATP hydrolysis. However, passive transfer of PLs from MlaFEDB to MlaC has also been
147 reported (31). To address this discrepancy, we also studied PL transfer in the anterograde direction using our
148 nanodisc-reconstituted complexes. We reconstituted MlaFEDB and MlaFEB complexes into nanodiscs containing
149 [^{14}C]-labelled PLs (Figure S7), and incubated these purified nanodiscs with tag-less apo MlaC. As negative control,
150 we showed that nanodiscs embedded MlaFEB transferred no or little PLs to MlaC (presumed non-specific transfer
151 up to ~5%) (Figure 5A and 5B). In the presence of MlaD, the MlaFEDB complex spontaneously transferred ~20% of
152 radioactive PLs from the nanodiscs to MlaC, supporting the possibility of anterograde transport (Figure 5A and 5C).
153 Remarkably, however, addition of ATP entirely prevented transfer of PLs from MlaFEDB to MlaC, and this
154 phenomenon was inhibited by addition of vanadate. Therefore, even though MlaD can spontaneously transfer PLs
155 to MlaC, ATP hydrolysis by the IM complex abolishes such activity.

156

157 **Discussion**

158 In this work, we have reconstituted ATP-powered retrograde PL transport mediated by the IM ABC
159 transporter of the OmpC-Mla system, using purified components. By applying [^{14}C]-labelled lipids, we have
160 demonstrated spontaneous PL transfer from MlaC to the MlaFEDB complex, with enhanced lipid transfer occurring
161 upon ATP hydrolysis (Figure 2). We have also observed spontaneous PL transfer from MlaFEDB to MlaC but this

162 transfer is abolished in the presence of ATP (Figure 5). Therefore, we have shown that PLs equilibrate between MlaC
163 and MlaFEDB, and ATP hydrolysis drives overall transport in the retrograde direction.

164 Here is a mechanistic model for MlaFEDB function, integrating all available biochemical and structural
165 information (Figure 6). In the first step, PL-bound MlaC arrives at the IM, and interacts with the MlaFEDB complex
166 via the protomer interfaces of MlaD hexamers (15). This ensues the reversible partitioning of the PL molecule(s)
167 between the lipid binding pockets of MlaC and the complex, even in the absence of ATP. While MlaD hexamers
168 alone bind PLs much less strongly than MlaC (15), the MlaFEDB complex, where several structures now reveal a
169 combined lipid binding cavity formed by both MlaD and MlaE (19-23), must possess strong affinity for PLs, likely
170 comparable to MlaC. The trajectory of PL movement between the two binding sites remains to be clarified. In the
171 second step, ATP binding has been shown to induce two conformational states of the MlaFEDB complex, believed
172 to be sequential in the process (21). Initial ATP binding to MlaF appears to cause a conformational change involving
173 upward movement of MlaD away from MlaE, which likely releases the PL molecule(s) from MlaD binding to be
174 eventually bound by MlaE alone. Subsequent complete binding of ATP induces tight dimerization of MlaF, in turn
175 collapsing the MlaE lipid binding cavity (21, 23), eventually forcing bound PL molecule(s) into the membrane. Whether
176 PLs enter the outer leaflet of the IM, or get flipped across the bilayer, is not known. In the final step, ATP hydrolysis
177 resets the MlaFEDB complex, allowing it to again adopt the nucleotide-free state. ATP binding and/or hydrolysis are
178 therefore required to overcome the energy barrier conferred by tight binding of PLs within the lipid binding cavity of
179 the MlaFEDB complex. Consistent with this model, MlaC itself is unable to activate ATPase activity (Figure S1B).
180 This whole ATP-driven process ultimately favors retrograde PL transfer from MlaC, via the MlaFEDB complex, to the
181 IM, in accordance with the Le Chatelier's principle.

182 In the context of the model, MlaD influences both the spontaneous and ATP-coupled steps of PL transfer.
183 We speculate that the conformational flexibility of MlaD hexamers plays a major role in achieving such modulation.
184 Unlike wildtype MlaD, the $MlaD_{\Delta 141\text{-}183}$ variant exists as hexamers in the complex that are not stable to SDS (Figure
185 S5), representing a "loose" form of the hexamer with greater conformational freedom. In support of this idea, the
186 soluble domain of this variant can form heptamers in vitro (14). The MlaFEDB complex with a "loose" MlaD hexamer
187 would have a more flexible lipid binding cavity, therefore incurring greater entropic costs to bind ligands. The
188 $MlaFED_{\Delta 141\text{-}183}B$ complex may thus have a lower affinity for PLs, resulting in reduced spontaneous PL transfer from

189 MlaC (Figure 4). Increased conformational flexibility may also account for the much higher ATPase activity of this
190 variant complex, possibly by facilitating conformational movements in the MlaE permease domains associated with
191 the ATP hydrolytic cycle; however, this led to uncoupling between ATP hydrolysis and PL transfer. By analogy, we
192 posit that the $MlaD_{L106N/L107N}$ variant forms "tight" hexamers in the complex, perhaps due to more hydrogen bonding
193 interactions in the central pore. Decreased conformational flexibility thereby confers an increase in affinity for
194 spontaneous PL binding and yet a reduced ATPase activity (Figure 4). Overall, we propose that the conformational
195 flexibility in the wildtype MlaD hexamer is optimally tuned to strike a balance between PL binding and ATPase activity,
196 yet ensure productive coupling between PL transfer and ATP hydrolysis. Still, MlaD mutations may also have direct
197 impact on PL binding enthalpies and/or interactions with MlaC. Further studies to test these ideas would be needed.
198 This reconstitution addresses the controversy of directionality, and establishes that ATP drives retrograde
199 PL transport mediated by the OmpC-Mla system. Our work thus validates the interpretation of OmpC-Mla function in
200 existing genetic studies (10, 11, 26, 27), and is consistent with plastid or mycobacterial homologs of the Mla IM
201 complex being characterized as lipid uptake systems (33-35). Our PL transfer assay demonstrates point-to-point
202 movement of native PLs between MlaC and MlaFEDB, and reveals both reversible spontaneous and irreversible
203 ATP-activated steps in the process. The existence of the spontaneous step, due to equilibration between the lipid
204 binding sites in MlaC and MlaFEDB, explains why an earlier report can detect "anterograde" PL transfer from the
205 liposome-reconstituted IM complex to MlaC (31). Yet, high sensitivity imparted by the use of [^{14}C]-labelled lipids
206 allowed us to identify the key role ATP hydrolysis play in ultimately driving PL transport in the retrograde fashion. In
207 the midst of preparing this manuscript, Tang et al. have independently developed an indirect assay using non-native
208 fluorescent lipids, and similarly reported that the Mla pathway mediates ATP-dependent retrograde PL transport in
209 vitro (20). While they did not detect the spontaneous retrograde step, our complementary assays collectively establish
210 the directionality of the system. Importantly, these PL transport assays serve as critical tools for detailed mechanistic
211 studies, and for future identification and validation of small molecule inhibitors against the OmpC-Mla pathway.
212 Adapted assays can also be applied to study possible lipid transport mediated by other putative systems, including
213 the Tol-Pal complex (30) and other MCE domain-containing complexes (14, 36, 37).

214 **Materials and Methods**

215 **Reconstitution of membrane proteins in lipid nanodiscs**

216 The reconstitutions of purified membrane proteins (MlaF(His-E)B, MlaF(His-E)DB, MlaF$_{K47A}$(His-E)DB,
217 MlaF(His-E)DB$_{T52A}$, MlaF(His-E)D$_{L106/L107N}$B and MlaF(His-E)D$_{\Delta 141-183}$B) into nanodiscs were adapted from published
218 protocols (18). 10 mg of *E. coli* polar lipid extracts (Avanti Polar Lipids) were dissolved in 1 mL of chloroform and
219 dried overnight. 1 mL of TBS buffer (20 mM Tris.HCl pH 8.0, 150 mM NaCl) containing 25 mM sodium cholate
220 (Sigma-Aldrich) was added to the dried lipid film, and vortexed and sonicated until a clear solution was obtained. The
221 respective Mla complex, the membrane scaffold protein MSP1E3D1-His and lipid were mixed at a molar ratio of
222 1:10:1500 in TBS and incubated, with rocking, for 1 h at 4 °C. Bio-beads SM2 resin (Bio-Rad) was subsequently
223 added to the solution (30 mg per 1-mL reconstitution mixture) and incubated with gentle agitation for 3 h at 4 °C.
224 Upon removal of Bio-beads, the sample was concentrated and purified by size exclusion chromatography (SEC) on
225 a Superose 6 Increase 10/300 GL column (GE Healthcare) on ÄKTA™ Pure. 0.5-mL fractions were collected and
226 subjected to SDS-PAGE analysis and Coomassie blue staining (InstantBlue™, expedeon). Fractions containing the
227 nanodisc-embedded complex were pooled and concentrated on a 30 kDa cut-off ultra-filtration device (Amicon Ultra,
228 Merck Millipore). For the reconstitution of radioactive nanodisc-embedded MlaF(His-E)B and MlaF(His-E)DB
229 complexes, [^{14}C]-labelled PLs extracted from [^{14}C]-acetate labelled cells were used in place of *E. coli* polar lipid
230 extracts, and the nanodiscs samples were purified on a self-packed column containing Superose 6 Prep Grade (GE
231 Healthcare) instead.

232

233 **In vitro PL transfer assays**

234 For in vitro retrograde PL transfer experiments, 10 μM of purified tag-less MlaC bound to [^{14}C]-labelled PLs
235 was incubated with 2 μM of purified non-radioactive His-tagged nanodisc-embedded complex. For in vitro
236 anterograde PL transfer experiments, 10 μM of purified tag-less apo MlaC was incubated with 2 μM of purified His-
237 tagged nanodisc-embedded complex reconstituted with [^{14}C]-labelled PLs. These components were incubated in 400
238 μL TBS buffer, either in the absence or presence of 2 mM ATP (Sigma-Aldrich) and 2 mM $MgCl_2$, for 10 min at 37°C.
239 After the transfer reaction, the mixture was topped up with TBS to a final volume of 2.5 mL, and incubated with 0.5
240 mL nickel resin (His60 Ni Superflow Resin, Takara Bio) in a Poly-Prep chromatography column (BioRad) for 1h, with

241 rocking, at room temperature. The filtrate (containing separated tag-less MlaC) was collected after the mixture was
242 passed through the resin twice. The resin was washed with 5 x 4 mL TBS containing 30 mM imidazole, and the
243 nanodisc-embedded complex was eluted with 2.5 mL TBS containing 300 mM imidazole. Samples obtained from the
244 nickel affinity-based separation were subjected to SDS-PAGE analysis and visualized by silver staining to ensure
245 that there was minimal cross-contamination of the two components. For experiments involving vanadate, 2 μM of the
246 nanodisc-embedded MlaFEDB complex was first pre-incubated with 2 mM ATP and 2 mM $MgCl_2$ for 5 min, then with
247 2.7 mM vanadate for 10 min, before finally incubating with 10 μM of MlaC for 10 min for PL transfer. 2 mM AMP-PNP
248 (Sigma-Aldrich) was also used in place of ATP for specific transfer experiments. All transfer experiments were
249 conducted in triplicates.

250 After separation of the filtrate (tag-less MlaC) and eluate (His-tagged nanodisc-embedded complex), 2 mL
251 of each component was added to 2 mL Ultima Gold scintillation fluid (PerkinElmer), and radioactivity counted on the
252 MicroBeta2 scintillation counter (PerkinElmer). The recovery of tag-less MlaC was quantified using the ratio standard
253 curve method (38) while that of His-tagged nanodisc-embedded complexes were quantified using the Lowry assay
254 (DC Protein Assay, Bio-Rad). For retrograde assay, the average gains and losses of radioactivity in the nanodiscs
255 and MlaC, respectively, were normalized to the initial [14C]-counts in MlaC using the following equation:

256 $$\text{Recovered radioactivity} = \frac{[14\text{C}]\text{ counts associated with sample}}{\frac{\text{Amount of sample recovered}}{\text{Initial amount of sample used}}} \times \frac{100\%}{\text{Initial count on MlaC}}$$

257 Fold changes in gains and losses of radioactivity in the nanodiscs and MlaC, respectively, were derived after
258 accounting for MlaFEB background and normalized to data from co-incubation of MlaFEDB/MlaC without ATP
259 (MlaFEDB (-ATP).

260 For the anterograde assay, the average gains and losses of radioactivity in the MlaC and nanodiscs,
261 respectively, were normalized to the initial [14C]-counts in nanodisc using the following equation:

262 $$\text{Recovered radioactivity} = \frac{[14\text{C}]\text{ counts associated with sample}}{\frac{\text{Amount of sample recovered}}{\text{Initial amount of sample used}}} \times \frac{100\%}{\text{Initial count on nanodisc}}$$

263

Acknowledgments

W.-Y.L. was supported by the National University of Singapore President's Graduate Fellowship (PGF). This work was supported by the Singapore Ministry of Health National Medical Research Council under its Open Fund Individual Research Grant (MOH-000145) (to S.-S.C.). The authors declare no conflict of interest.

References

1. Y. Kamio, H. Nikaido, Outer membrane of *Salmonella typhimurium*: accessibility of phospholipid head groups to phospholipase C and cyanogen bromide activated dextran in the external medium. *Biochem.* 15, 2561-2570 (1976).
2. H. Nikaido, Molecular basis of bacterial outer membrane permeability revisited. *Microbiol. Mol. Biol. Rev.* 67, 593-656 (2003).
3. S. Okuda, H. Tokuda, Lipoprotein sorting in bacteria. *Annu. Rev. Microbiol.* 65, 239-259 (2011).
4. P. Sperandeo, A. M. Martorana, A. Polissi, Lipopolysaccharide biogenesis and transport at the outer membrane of Gram-negative bacteria. *Biochim. Biophys. Acta.* 1862, 1451-1460 (2017).
5. N. Noinaj, J. C. Gumbart, S. K. Buchanan, The beta-barrel assembly machinery in motion. *Nat. Rev. Microbiol.* 15, 197-204 (2017).
6. R. Shrivastava, S.-S. Chng, Lipid trafficking across the Gram-negative cell envelope. *J. Biol. Chem.* 294, 14175-14184 (2019).
7. A. M. Donohue-Rolfe, M. Schaechter, Translocation of phospholipids from the inner to the outer membrane of Escherichia coli. *Proc. Natl. Acad. Sci. U.S.A.* 77, 1867-1871 (1980).
8. N. C. Jones, M. J. Osborn, Translocation of phospholipids between the outer and inner membranes of Salmonella typhimurium. *J Biol Chem* 252, 7405-7412 (1977).
9. K.E. Langley, E. Hawrot, E.P. Kennedy, Membrane assembly: movement of phosphatidylserine between the cytoplasmic and outer membranes of Escherichia coli. *J. Bacteriol.* 152, 1033–1041 (1982).
10. J. C. Malinverni, T. J. Silhavy, An ABC transport system that maintains lipid asymmetry in the Gram-negative outer membrane. *Proc. Natl. Acad. Sci. U.S.A.* 106, 8009-8014 (2009).

290 11. Z.-S. Chong, W.-F. Woo, S.-S. Chng, Osmoporin OmpC forms a complex with MlaA to maintain outer
291 membrane lipid asymmetry in Escherichia coli. *Mol. Microbiol.* 98, 1133-1146 (2015).
292 12. J. Yeow *et al.*, The architecture of the OmpC-MlaA complex sheds light on the maintenance of outer
293 membrane lipid asymmetry in Escherichia coli. *J. Biol. Chem.* 293, 11325-11340 (2018).
294 13. J. Abellon-Ruiz *et al.*, Structural basis for maintenance of bacterial outer membrane lipid asymmetry. *Nat.*
295 *Microbiol.* 2, 1616-1623 (2017).
296 14. D. C. Ekiert *et al.*, Architectures of Lipid Transport Systems for the Bacterial Outer Membrane. *Cell* 169, 273-
297 285 e217 (2017).
298 15. B. Ercan, W.-Y. Low, X. Liu, S.-S. Chng, Characterization of Interactions and Phospholipid Transfer between
299 Substrate Binding Proteins of the OmpC-Mla System. *Biochem.* 58, 114-119 (2019).
300 16. D. Yero *et al.*, The Pseudomonas aeruginosa substrate-binding protein Ttg2D functions as a general
301 glycerophospholipid transporter across the periplasm. *Commun. Biol.* 4, 448 (2021).
302 17. G. L. Isom *et al.*, MCE domain proteins: conserved inner membrane lipid-binding proteins required for outer
303 membrane homeostasis. *Sci. Rep.* 7, 8608 (2017).
304 18. S. Thong *et al.*, Defining key roles for auxiliary proteins in an ABC transporter that maintains bacterial outer
305 membrane lipid asymmetry. *Elife* 5, e19042 (2016).
306 19. N. Coudray *et al.*, Structure of bacterial phospholipid transporter MlaFEDB with substrate bound. *Elife* 9,
307 e62518 (2020).
308 20. X. Tang *et al.*, Structural insights into outer membrane asymmetry maintenance in Gram-negative bacteria
309 by MlaFEDB. *Nat. Struct. Mol. Biol.* 28, 81-91 (2021).
310 21. X. Chi *et al.*, Structural mechanism of phospholipids translocation by MlaFEDB complex. *Cell Res.* 30, 1127-
311 1135 (2020).
312 22. C. Zhou *et al.*, Structural Insight into Phospholipid Transport by the MlaFEBD Complex from P. aeruginosa.
313 *J. Mol. Biol.* 433, 166986 (2021).
314 23. Y. Zhang, Q. Fan, X. Chi, Q. Zhou, Y. Li, Cryo-EM structures of Acinetobacter baumannii glycerophospholipid
315 transporter. *Cell Discov.* 6, 86 (2020).

316 24. L. Aravind, E.V. Koonin, The STAS domain - a link between anion transporters and antisigma-factor
317 antagonists. *Curr. Biol.* 10, R53–R55 (2000).
318 25. L. R. Kolich *et al.*, Structure of MlaFB uncovers novel mechanisms of ABC transporter regulation. *Elife* 9,
319 e60030 (2020).
320 26. M. J. Powers, M. S. Trent, Phospholipid retention in the absence of asymmetry strengthens the outer
321 membrane permeability barrier to last-resort antibiotics. *Proc. Natl. Acad. Sci. U.S.A.* 115, E8518-E8527
322 (2018).
323 27. E. Nagy, R. Losick, D. Kahne, Robust suppression of lipopolysaccharide deficiency in *Acinetobacter*
324 *baumannii* by growth in minimal Mmedium**.** *J. Bacteriol.* 201, e00420-19 (2020).
325 28. C. Kamischke *et al.*, The Acinetobacter baumannii Mla system and glycerophospholipid transport to the outer
326 membrane. *Elife* 8, e40171 (2019).
327 29. M. J. Powers, B. W. Simpson, M. S. Trent, The Mla pathway in Acinetobacter baumannii has no
328 demonstrable role in anterograde lipid transport. *Elife* 9, e56571 (2020).
329 30. R. Shrivastava, X. Jiang, S.-S. Chng, Outer membrane lipid homeostasis via retrograde phospholipid
330 transport in Escherichia coli. *Mol. Microbiol.* 106, 395-408 (2017).
331 31. G. W. Hughes *et al.*, Evidence for phospholipid export from the bacterial inner membrane by the Mla ABC
332 transport system. *Nat. Microbiol.* 4, 1692-1705 (2019).
333 32. T. K. Ritchie *et al.*, Reconstitution of membrane proteins in phospholipid bilayer nanodiscs. *Methods*
334 *enzymo*l. 464, 211-231 (2009).
335 33. C. Benning, Mechanisms of lipid transport involved in organelle biogenesis in plant cells. *Annu. Rev. Cell*
336 *Dev. Biol.* 25, 71-91 (2009).
337 34. A. K. Pandey, C. M. Sassetti, Mycobacterial persistence requires the utilization of host cholesterol. *Proc.*
338 *Natl. Acad. Sci. U.S.A.* 105, 4376-4380 (2008).
339 35. S. A. Cantrell *et al.*, Free mycolic acid accumulation in the cell wall of the mce1 operon mutant strain of
340 Mycobacterium tuberculosis. *J. Microbiol.* 51, 619-626 (2013).
341 36. G. L. Isom *et al.*, LetB Structure Reveals a Tunnel for Lipid Transport across the Bacterial Envelope. *Cell*
342 181, 653-664 e619 (2020)

343 37. C. Liu, J. Ma, J. Wang, H. Wang, L. Zhang, Cryo-EM Structure of a Bacterial Lipid Transporter YebT. *J. Mol.*
344 *Biol.* 432, 1008-1019 (2020).
345 38. A. Pitre, Y. Pan, S. Pruett, O. Skalli, On the use of ratio standard curves to accurately quantitate relative
346 changes in protein levels by western blot. *Anal. Biochem.* 361, 305-307 (2007).

347 **Figures**

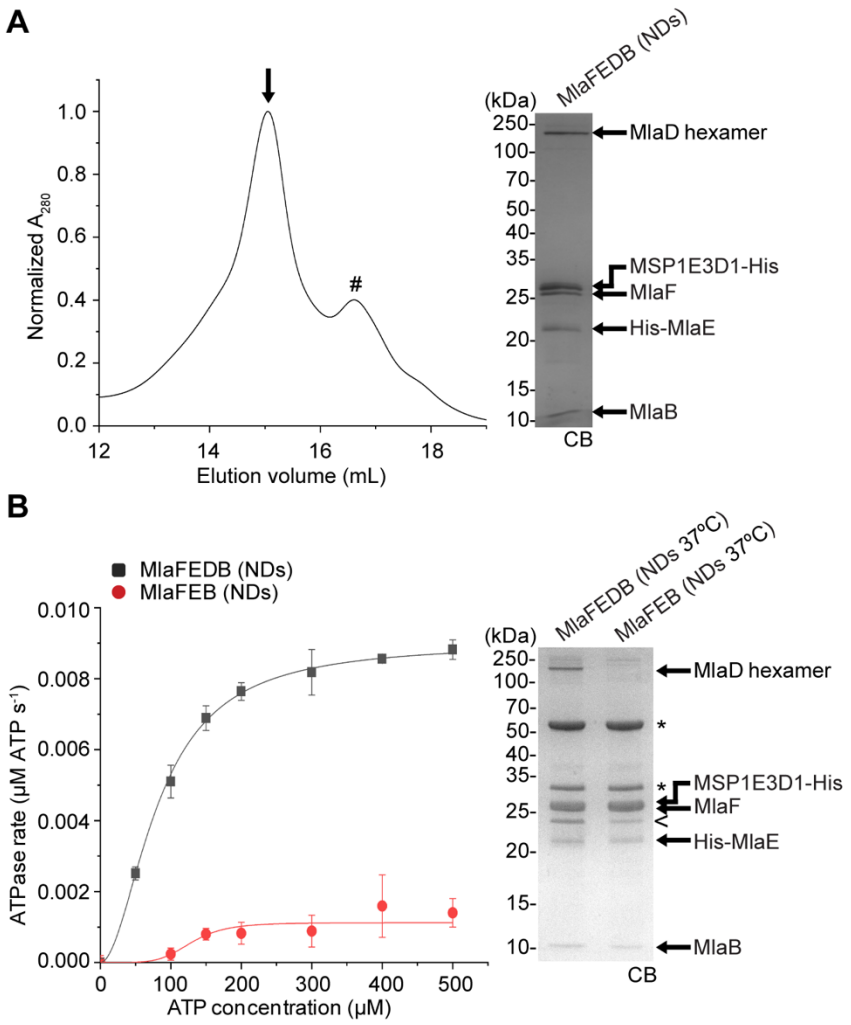

348

349 **Figure 1.** Nanodisc-embedded MlaFEDB exhibits higher ATP hydrolytic activity than MlaFEB. (A) Size-exclusion
350 chromatographic profile of nanodisc-reconstituted (NDs) MlaFEDB complex. SDS-PAGE analysis of the peak fraction
351 (annotated with an arrow (↓)) is shown on the right. #, empty NDs. (B) Enzyme-coupled ATPase assays of nanodisc-
352 embedded MlaFEDB and MlaFEB complexes (0.1 μM) at 37°C. Average ATP hydrolysis rates from triplicate
353 experiments were plotted against ATP concentrations, and fitted to an expanded Michaelis-Menten equation that
354 includes a term for Hill coefficient (n); MlaFEDB NDs (k_{cat} = Vmax/[complex] = 0.090 ± 0.002 μmol ATP s^{-1}/μmol
355 complex, K_m = 82.5 ± 4.3 μM, n = 1.9 ± 0.2) and MlaFEB NDs (k_{cat} = 0.011 ± 0.002 μmol ATP s^{-1}/μmol complex, K_m
356 = 129.1 ± 12.8 μM, n = 5.3 ± 2.0). Errors depicted by bars and ± signs are standard deviations of triplicate data. SDS-

357 PAGE analysis of the complexes used for these assays is shown on the right. *, pyruvate kinase/lactate
358 dehydrogenase enzymes used in coupled assay; <, degraded MSP1E3D1. CB, Coomassie blue staining.

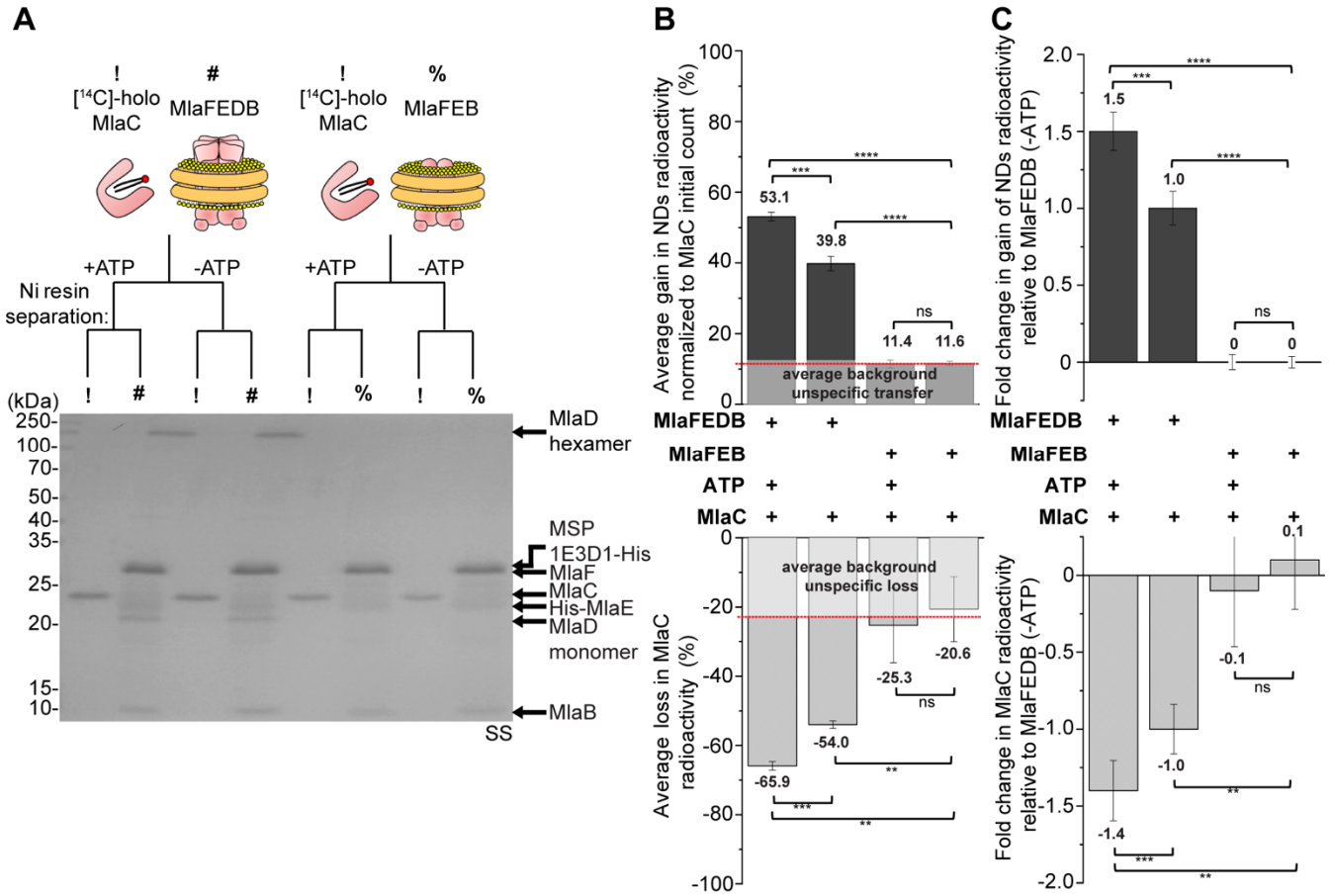

Figure 2. MlaC transfers [^{14}C]-labelled lipids to nanodisc-embedded MlaFEDB in an MlaD- and ATP-dependent manner. (A) SDS-PAGE analysis of indicated samples following co-incubation with or without ATP, and subsequent nickel affinity-based clean separation of tag-less [^{14}C]-PL bound (holo) MlaC (10 μM) and His-tagged non-radioactive nanodisc-embedded complexes (2 μM). SS, silver staining. (B) Average gains and losses of radioactivity ([^{14}C]-lipids) in the indicated nanodiscs (*top*) and MlaC (*bottom*), respectively, normalized to the initial counts on MlaC. Data from co-incubation of MlaFEB/MlaC are treated as unspecific background transfer/loss. (C) Fold changes in gains and losses of radioactivity in the indicated nanodiscs (*top*) and MlaC (*bottom*), respectively, derived from (B) after accounting for MlaFEB background and normalized to data from co-incubation of MlaFEDB/MlaC without ATP (MlaFEDB (-ATP)). Error bars represent standard deviations calculated from triplicate experiments. Student's t-tests: ns, not significant; **, $p < 0.01$; ***, $p < 0.001$, ****; $p < 0.0001$.

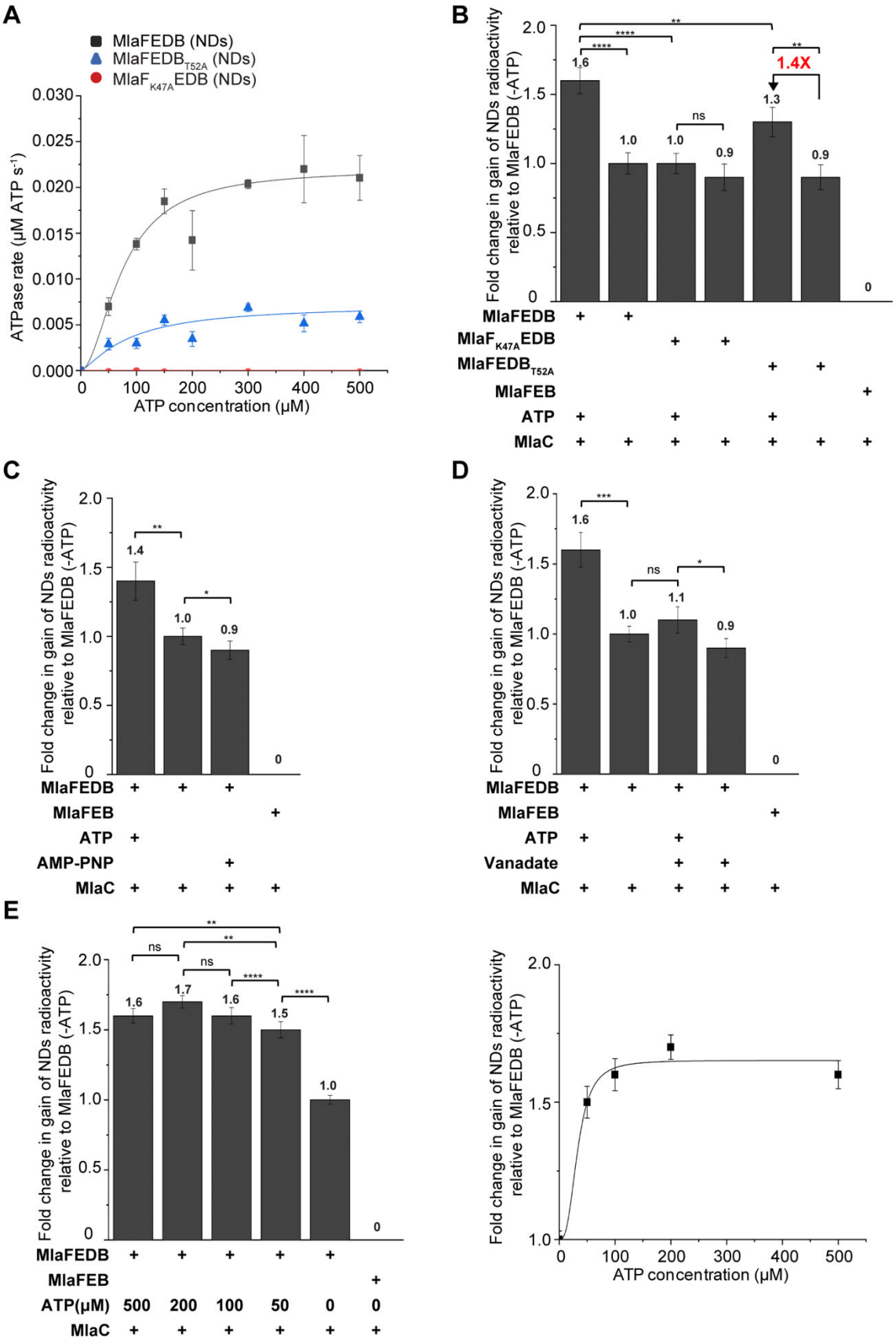
A
MlaFEDB (NDs)
MlaFEDB$_{T52A}$ (NDs)
MlaF$_{K47A}$EDB (NDs)
ATPase rate (μM ATP s^{-1})
ATP concentration (μM)
B
Fold change in gain of NDs radioactivity relative to MlaFEDB (-ATP)
1.4X
MlaFEDB
MlaF$_{K47A}$EDB
MlaFEDB$_{T52A}$
MlaFEB
ATP
MlaC
C
Fold change in gain of NDs radioactivity relative to MlaFEDB (-ATP)
MlaFEDB
MlaFEB
ATP
AMP-PNP
MlaC
D
Fold change in gain of NDs radioactivity relative to MlaFEDB (-ATP)
MlaFEDB
MlaFEB
ATP
Vanadate
MlaC
E
Fold change in gain of NDs radioactivity relative to MlaFEDB (-ATP)
MlaFEDB
MlaFEB
ATP(μM)
MlaC
Fold change in gain of NDs radioactivity relative to MlaFEDB (-ATP)
ATP concentration (μM)

370

371 **Figure 3.** ATP hydrolysis is coupled to retrograde PL transport. (A) Enzyme-coupled ATPase assays of nanodisc-
372 embedded MlaFEDB, MlaFEDB$_{T52A}$ and MlaF$_{K47A}$EDB complexes (0.1 μM) at 37°C. Average ATP hydrolysis rates
373 from triplicate experiments were plotted against ATP concentrations, and fitted to an expanded Michaelis-Menten
374 equation that includes a term for Hill coefficient (n); MlaFEDB NDs (k_{cat} = 0.220 ± 0.000 μmol ATP s^{-1}/μmol complex,
375 K_m = 75.0 ± 8.0 μM, n = 1.9 ± 0.4), MlaFEDB$_{T52A}$ NDs (k_{cat} = 0.072 ± 0.028 μmol ATP s^{-1}/μmol complex, K_m = 88.4 ±
376 62.1 μM, n = 1.3 ± 1.2). SDS-PAGE analysis of the complexes used for the assay is shown in Figure S3A. (B-E) Fold
377 changes in gains of radioactivity ([^{14}C]-lipids) in indicated nanodiscs, following co-incubation and subsequent nickel
378 affinity-based separation of tag-less [^{14}C]-PL bound (holo) MlaC (10 μM) and His-tagged non-radioactive nanodisc-
379 embedded complexes (2 μM), for (B) ATPase mutant complexes, (C) addition of AMP-PNP, (D) addition of vanadate
380 (2.7 mM), and (E) different ATP concentrations. Data from (E) are replotted on the right and fitted to an expanded
381 Michaelis-Menten equation that includes a term for Hill coefficient (n); MlaFEDB NDs (K_m for ATP during PL transfer
382 = 33.1 ± 22.2 μM, n = 2.8 ± 4.6). SDS-PAGE analyses depicting clean separation of nanodisc-embedded complexes
383 and MlaC are shown in Figure S3B-E. Fold changes are derived from average gains in radioactivity counts in
384 indicated nanodiscs, after accounting for MlaFEB background and normalized to data from MlaFEDB (-ATP). Errors
385 depicted by bars and ± signs are standard deviations from triplicate data. Student's t-tests: ns, not significant; *, $p < 0.05$;
386 **, $p < 0.01$; ***, $p < 0.001$; ****, $p < 0.0001$.

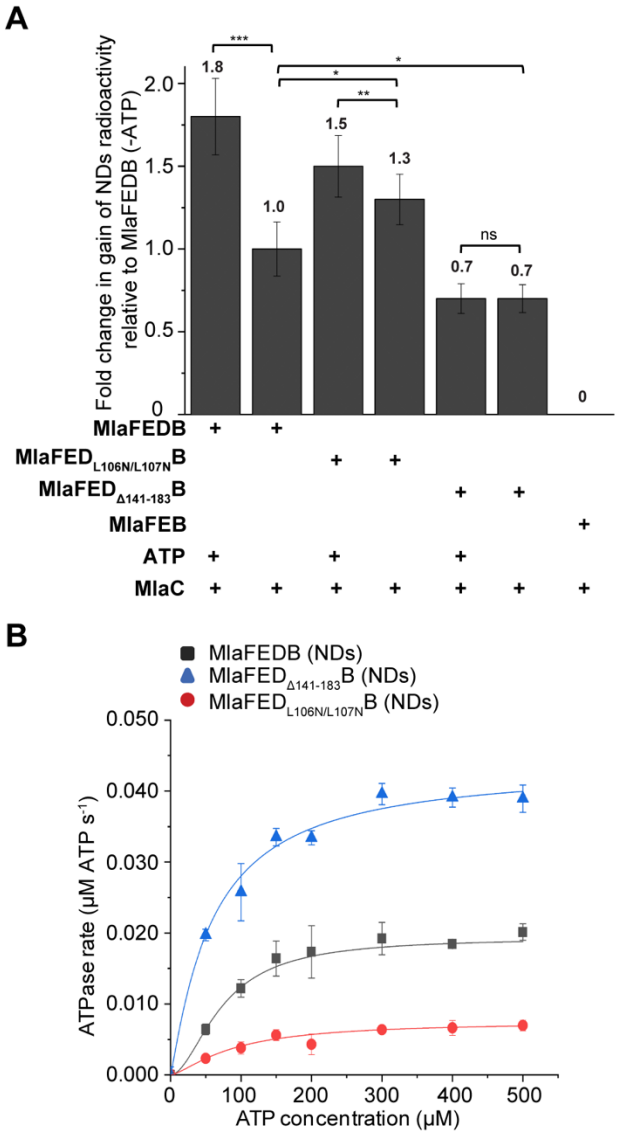

Figure 4. MlaD modulates both the spontaneous and ATP-activated PL transfer steps. (A) Fold changes in gains of radioactivity ([^{14}C]-lipids) in indicated nanodiscs, following co-incubation and subsequent nickel affinity-based separation of tag-less [^{14}C]-PL bound (holo) MlaC (10 μM) and His-tagged non-radioactive nanodisc-embedded complexes containing MlaD variants (2 μM). SDS-PAGE analyses depicting clean separation of nanodisc-embedded complexes and MlaC are shown in Figure S6A. Fold changes are derived from average gains in radioactivity counts in indicated nanodiscs, after accounting for MlaFEB background and normalized to data from MlaFEDB (-ATP). (B) Enzyme-coupled ATPase assays of nanodisc-embedded MlaFEDB, MlaFED$_{L106N/L107N}$B and MlaFED$_{\Delta141-183}$B complexes (0.1 μM) at 37°C. Average ATP hydrolysis rates from triplicate experiments were plotted against ATP

396 concentrations, and fitted to an expanded Michaelis-Menten equation that includes a term for Hill coefficient (n);
397 MlaFEDB NDs (k_{cat} = 0.193 ± 0.007 μmol ATP s^{-1}/μmol complex, K_m = 73.2 ± 6.9 μM, n = 1.8 ± 0.4),
398 MlaFED$_{L106N/L107N}$B NDs (k_{cat} = 0.075 ± 0.011 μmol ATP s^{-1}/μmol complex, K_m = 88.7 ± 26.3 μM, n = 1.4 ± 0.5) and
399 MlaFED$_{\Delta 141-183}$B NDs (k_{cat} = 0.436 ± 0.027 μmol ATP s^{-1}/μmol complex, K_m = 59.2 ± 7.5 μM, n = 1.1 ± 0.2). SDS-
400 PAGE analysis of the complexes used for the assay is shown in Figure S6B. Errors depicted by bars and ± signs are
401 standard deviations from triplicate data. Student's t-tests: ns, not significant; *, $p < 0.05$; **, $p < 0.01$; ***, $p < 0.001$.

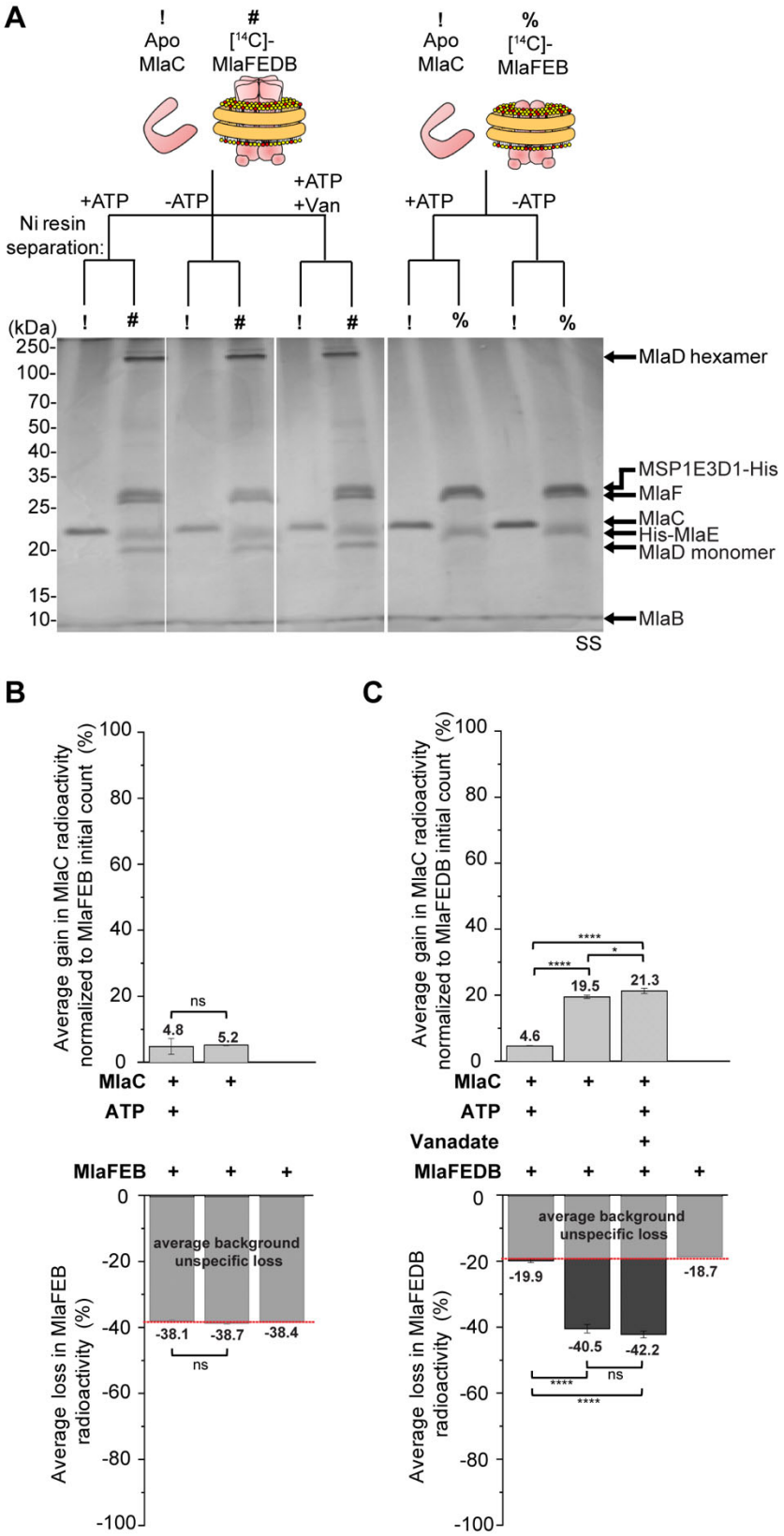
A
! Apo MlaC
[14C]-MlaFEDB
! Apo MlaC
% [14C]-MlaFEB
+ATP
-ATP
+ATP +Van
+ATP
-ATP
Ni resin separation:
(kDa)
250-
100-
70-
50-
40-
35-
25-
20-
15-
10-
MlaD hexamer
MSP1E3D1-His
MlaF
MlaC
His-MlaE
MlaD monomer
MlaB
SS
B
Average gain in MlaC radioactivity normalized to MlaFEB initial count (%)
ns
4.8
5.2
MlaC
ATP
MlaFEB
average background unspecific loss
-38.1
-38.7
-38.4
ns
Average loss in MlaFEB radioactivity (%)
C
Average gain in MlaC radioactivity normalized to MlaFEDB initial count (%)
****
*
****
4.6
19.5
21.3
MlaC
ATP
Vanadate
MlaFEDB
average background unspecific loss
-19.9
-40.5
-42.2
-18.7
****
ns
****
Average loss in MlaFEDB radioactivity (%)

402

403 **Figure 5.** ATP hydrolysis abolishes spontaneous transfer of PLs from MlaFEDB to MlaC. (A) SDS-PAGE analysis of
404 indicated samples following co-incubation with or without ATP, or vanadate, and subsequent nickel affinity-based
405 clean separation of tag-less non-radioactive apo MlaC (10 μM) and His-tagged nanodisc-embedded complexes
406 reconstituted with [^{14}C]-PLs (2 μM). SS, silver staining. (B) Average gains and losses of radioactivity ([^{14}C]-lipids) in
407 MlaC (*top*) and MlaFEB (*bottom*), respectively, normalized to the initial counts on MlaFEB. (C) Average gains and
408 losses of radioactivity ([^{14}C]-lipids) in MlaC (*top*) and MlaFEDB (*bottom*), respectively, normalized to the initial counts
409 on MlaFEDB. Data from co-incubation of MlaFEB/MlaFEDB with nickel resin alone are treated as unspecific
410 background loss. Error bars represent standard deviations calculated from triplicate experiments. Student's t-tests:
411 ns, not significant; *, $p < 0.05$; ****; $p < 0.0001$.

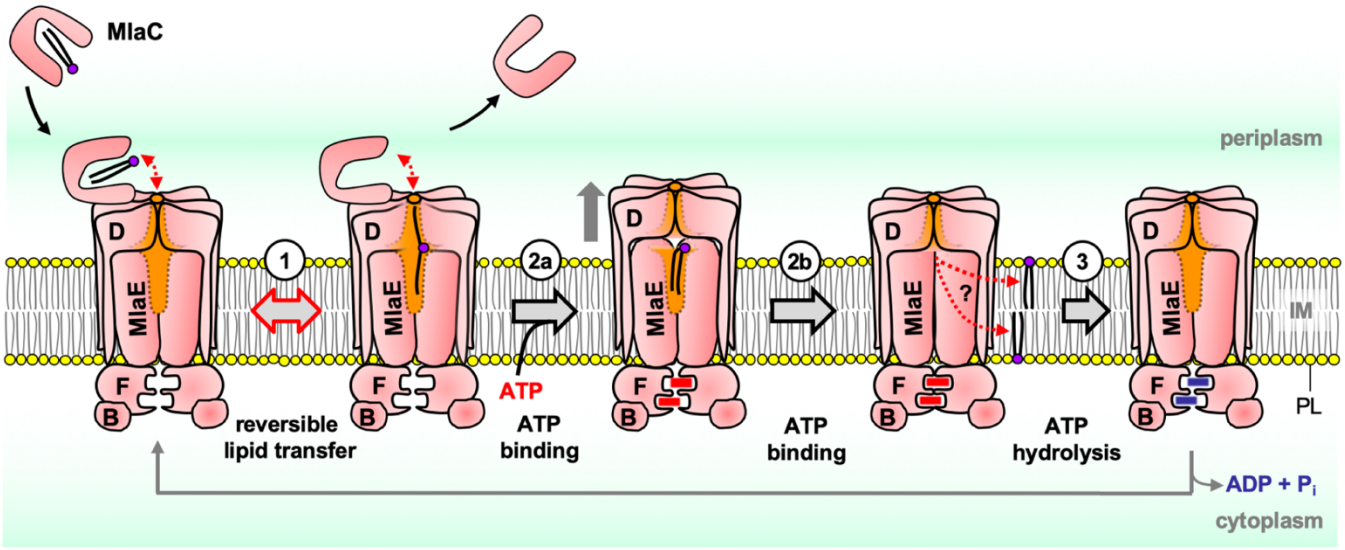

Figure 6. Proposed mechanistic model for MlaFEDB function in retrograde PL transfer. Step 1: Upon MlaC binding, reversible spontaneous transfer of PL cargo occurs between the lipid binding pocket in MlaC and the lipid binding cavity formed by both MlaD and MlaE in the complex (illustrated in orange). Step 2a: Initial ATP binding to MlaF may induce a state where MlaD moves away from MlaE (illustrated by grey arrow), possibly facilitating lipid binding by MlaE alone (21). Step 2b: Complete ATP binding eventually causes dimerization of MlaF, along with the collapse of the lipid binding cavity in MlaE, thus forcing the PL molecule into the membrane (21, 23). It is not clear which leaflet of the IM the PL molecule goes into. Step 3: Hydrolysis of ATP then resets such conformational changes, so the complex can return to the nucleotide apo state.